Proceedings of the 4th International Conference on Fluid Flow and Thermal Science (ICFFTS'23)
Lisbon, Portugal- December 07 - 09, 2023
Paper No. 161
DOI: 10.11159/icffts23.161

Phase Change Material Simulation for Electronics Cooling: A Comprehensive Validation and Verification of the Lattice Boltzmann Method

Anas Ghannam[1], Anas AlAzzam[1,2], Eiyad Abu-Nada[1]
[1]Department of Mechanical Engineering, Khalifa University of Science and Technology
[2]System on Chip Lab, Khalifa University of Science and Technology
Abu Dhabi, United Arab Emirates
anas.alazzam@ku.ac.ae; eiyad.abunada@ku.ac.ae

Abstract **-** In the realm of electronics cooling, ensuring efficient thermal management for high-heat electronic devices remains a pivotal challenge, particularly in light of the continuous advancement of microchip technology. This paper embarks on a concept to establish an optimal solution through the application of Phase Change Materials (PCMs). However, the complexity inherent in phenomena like Phase Change Material (PCM) melting poses a formidable obstacle for conventional Navier-Stokes equation solvers. Hence, the present work employs the Lattice Boltzmann (LB) method using the single relaxation Double Distribution Function (DDF). Such an approach is rigorously validated and verified with classical test cases, including Stefan's conduction melting and Gallium melting experiments. These analyses serve as a test, offering a comprehensive assessment of the method's performance. The results affirm the adaptability and competence of the model in handling mushy zones during PCM melting, demonstrating its efficacy in both one-dimensional and two-dimensional melting scenarios. This study paves the way for the implementation of efficient thermal management systems for high-heat electronic devices, underscoring the potential of the LB method in addressing the intricate challenges of PCM-based cooling strategies in the context of advancing chip technology.

Keywords**:** Phase Change Material, Lattice Boltzmann Method, Validation, Verification

1. Introduction

The demand in the chip industry is increasing at a high pace for electronic devices such as data centers, military equipment, electronic vehicles, photovoltaic solar cells, and light-emitting diodes; consequently, the industry engages more in the development of potent and efficient microchips. The deliberate selection of microchips on any other component as the focal point of attention arises from the pivotal role played by these microchips, which function as the central processing unit of the device and are responsible for executing a multitude of critical tasks encompassing data management and information processing. Such a statement suggests that the performance of electronic devices relies on the execution ability of the chip. However, microchips are constrained by the operating temperature which imposes a bottleneck because microchips are mainly Silicon semiconductors that are temperature-dependent. Moreover, according to Moore's law, an empirical estimation has dictated that the implementation of components on chips is doubled every two years [1]. Thus, integrating more transistors in chips for more computational power for thin devices will increase the power density of the chip and hence release higher heat flux with a magnitude of 1 MW/m^2 [2]. Because of all the above reasons, electronic devices primarily fail from high operating temperatures, which is a significant cause of failure in 55% [3] of all cases. As a result, great challenges arise to thermal management technologies to maintain the device's operations.

As previously mentioned, the dilemma of establishing powerful microchips while concurrently ensuring operational viability raised awareness in the area of thermal management systems. Various approaches have emerged for the goal of cooling electronic devices. To this date, numerous studies have been developed, indicating the importance of the study. The optimum thermal management system for cooling electronic devices must provide uniformity of the surface temperature and eliminate the local heating spots. In addition, mobile devices such as laptops and phones are thin, thus constraining the thermal management system space-wise. The ability of the cooling system to work passively is another benefit researchers are looking for when designing a cooling scheme.

The current literature [4] developed various emerging practices in the application of electronics cooling such as spray cooling, emersion cooling, microchannels, vortex generators, nanofluids, thermosyphons, phase change material (PCM), and heat pipes. Table 1 is constructed to pinpoint each of these approach's advantages, and shortcomings.

Table 1: A comparison between the benefits and shortcomings of the emerging cooling schemes.

Cooling Scheme	**Spray cooling**	**Emersion cooling**	**Microchannel**	**Vortex generator**	**Nanofluid**	**Thermosyphon**	**Phase Change Material (PCM)**	**Heat pipe**
Advantages	Achieves uniformity of surface temperature	Engulfs the heating element with the coolant for enhanced heat transfer	It is a two-phase flow and applies to miniaturized devices	It's a simple method to incorporate mixing and distribution of boundary layer	It increases the thermal conductivity of the base fluid	Simple, cheap, and does not require a pumping device	Has high latent heat of melting	Simple, practical, and applicable for miniaturized devices
Disadvantages	External pumping power is required	The coolant has poor thermal properties and needs sufficient space	External pumping power is required	The implementation causes an increase in pressure drop	The implementation causes an increase in pumping power	Not applicable to mobile electronic devices due to its dependence on gravity	It has low thermal conductivity and can leak in liquid form	A dry-out is a major issue in the cooling method

The comparison reveals essential information about the current cooling schemes, wherein the adoption of any of the aforementioned technologies is expected to manifest a significant drawback, consequently constraining the method's potential. Hence, the adaptation of two or more technologies together to surpass the original potential is implemented. The most prominent combination of the two technologies is the phase change material (PCM) with microchannel. The integration of PCM into microchannel represents a cutting-edge approach in electronics cooling. This innovative technology harnesses the exceptional heat absorption and release capabilities of PCMs during phase changes, ensuring efficient temperature control for electronic components. Microchannels, with their compact design, enable the precise distribution of PCMs, facilitating optimal thermal contact with the electronics. By regulating temperatures, PCMs not only enhance component reliability but also reduce the reliance on energy-intensive active cooling methods.

To examine the potential of this combination, a computational method should be carefully selected to accomplish accurate and appropriate findings. The complex phenomena of simulating phase change simulation, present challenges for traditional Navier-Stokes Equation (NSE) solvers. Especially, tracking the complex solid-liquid interface, which requires additional treatment in certain CFD packages. Such complexities are inherently handled by a discrete-type simulation approach called the Lattice Boltzmann Method (LBM). LBM excels in modeling phase change due to its simplicity in handling complex interfaces, efficient parallelizability, and natural alignment with the mesoscopic nature of phase change phenomena. This method offers ease of implementation and adaptability to multiphysics scenarios. Therefore, LBM is employed in this study to accurately replicate the real-life behavior of phase change material by validating and verifying the present study model. In this paper, the LB framework employed is OpenLB [5], coded in C++, and with a release version of 1.5.

2. Research Methodology

In this work, the simulation of the model is based on the single relaxation double distribution enthalpy-based LBE to to fully capture the transition between distinct phases and the sharp interference in the mushy zone. The general governing governing equations are first described in Section 2.1. Afterward, the discretized LB equation is defined with the enthalpy enthalpy distribution functions with a single relaxation coefficient established.

2.1. Governing Equations

The continuity, momentum, and energy equations describing the transient weakly compressible melting of PCMs are identified as the following in the tensor form:

$$\frac{\partial \rho}{\partial t} + \nabla \cdot (\rho \boldsymbol{u}) = 0 \tag{01}$$

$$\frac{\partial (\rho \boldsymbol{u})}{\partial t} + \nabla \cdot (\rho \boldsymbol{u}\boldsymbol{u}) = -\nabla \mathrm{p} + \mu(\nabla^2 \boldsymbol{u}) + \boldsymbol{F} \tag{02}$$

$$\frac{\partial (\rho H)}{\partial t} = -\nabla \cdot \left(\rho \mathrm{C}_p \mathrm{T} \boldsymbol{u}\right) + \kappa(\nabla^2 \mathrm{T}) \tag{03}$$

where t, ρ, $\boldsymbol{u}$, p, $\boldsymbol{F}$, H, C_p, κ, and T represent time, density, velocity, pressure, buoyancy force, enthalpy, specific heat capacity, thermal conductivity and temperature, respectively. The buoyancy force is estimated using the Boussinesq approximation $\left[\boldsymbol{F} = \rho\beta g(T - T_{ref})\right]$ where β, g, and T_{ref} are the volumetric thermal expansion, gravitational acceleration, and the reference temperature, respectively. The enthalpy is then obtained by the summation of the sensible heat $\mathrm{C}_p T$ and the latent heat $f_l L$. Here, f_l represents the liquid fraction and L is the latent heat of melting.

2.2. Lattice Boltzmann Method

The Lattice Boltzmann Equation is a discretized form of the Boltzmann transport equation leading to the formation of the density distribution function for the fluid flow where the governing equations Eqs. (1) - (3) are recovered from Eq. (4) through the Chapman–Enskog expansion. For the simulation of PCM, Noble and Torczynski [6] introduced the partially saturated method for tracing and adapting to the moving interface. Therefore, the density distribution function f_i is given as:

$$f_i(x + \boldsymbol{c_i}\Delta t, t + \Delta t) = f_i(x,t) + B\Omega_i^s(x,t) + (1 - B)\Omega_i^f(x,t) + \boldsymbol{F}_i \tag{04}$$

$$B(x,t) = \frac{(1 - f_l(x,t))\left(\frac{\tau_f}{\Delta t} - \frac{1}{2}\right)}{f_l(x,t) + \left(\frac{\tau_f}{\Delta t} - \frac{1}{2}\right)} \tag{05}$$

where B is the weighting function to distinguish between solid and liquid interfaces. When the liquid fraction f_l is 1, then the conventional density distribution function for a fluid is obtained. τ_f and $\boldsymbol{F}_i$ are the relaxation time and external forces acting on the fictitious particles. The term on the left describes the streaming of particles during the time step Δt and the right-hand side term Ω_i represents the collision operator with superscript f and s representing the fluid and solid given as:

$$\Omega_i^f(x,t) = \frac{\Delta t}{\tau_f}\left(f_i^{eq}(\rho_f, t) - f_i(x,t)\right) \tag{06}$$

$$\Omega_i^s(x,t) = \left(f_i^{eq}(\rho, \boldsymbol{u_s}) - f_i(x,t)\right) + \left(1 - \frac{\Delta t}{\tau_f}\right)\left(f_i(x,t) - f_i^{eq}(\rho, \boldsymbol{u})\right) \tag{07}$$

where the solid velocity $\boldsymbol{u_s}$ is equal to zero. The equilibrium distribution function ${f_i}^{eq}$ and the relaxation time are specified by:

$$ {f_i}^{eq} = \omega_i \rho \left(1 + \frac{\boldsymbol{u} \cdot \boldsymbol{c_i}}{{c_s}^2} + \frac{(\boldsymbol{u} \cdot \boldsymbol{c_i})^2}{2{c_s}^4} - \frac{\boldsymbol{u} \cdot \boldsymbol{u}}{2{c_s}^2} \right) \tag{08} $$

$$ \tau_f = \frac{\nu}{{c_s}^2} + 0.5\Delta t \tag{09} $$

where ω_i, ν, $\boldsymbol{c_i}$ and c_s are the weight coefficient, kinematic viscosity, discrete velocity in the direction of *i* and the speed of sound. Using the above equations, the macroscopic density, pressure and momentum are calculated from the below equations:

$$ \rho(x,t) = \sum_{i=0}^{Q-1} f_i(x,t) \tag{10} $$

$$ p = \sum_{i=0}^{Q-1} {c_s}^2 \cdot f_i(x,t) \tag{11} $$

$$ \boldsymbol{u}(x,t) = \frac{1}{\rho} \sum_{i=0}^{Q-1} \boldsymbol{c_i} f_i(x,t) \tag{12} $$

Here Q represents the total possible discrete obtained from the velocity set selected. The second distribution function, responsible for handling the thermal behavior is proposed by Haung, Wu, and Cheng [7] which is intended to solve the equation using a single relaxation collision scheme in which it describes the distribution function g_i as:

$$ g_i(x + \boldsymbol{c_i}\Delta t, t + \Delta t) = g_i(x,t) - \frac{\Delta t}{\tau_g}(g_i(x,t) - {g_i}^{eq}(x,t)) \tag{13} $$

where ${g_i}^{eq}$ is the equilibrium distribution function, and τ_g is the dimensionless thermal relaxation time given as $\left[\tau_g = \alpha/{c_s}^2 + 0.5\Delta t\right]$ in which α is the thermal diffusivity $\left[\alpha = \kappa/\rho \mathrm{C}_{p,ref}\right]$. The reference specific heat capacity is represented by $\mathrm{C}_{p,ref}$. The equilibrium distribution function ${g_i}^{eq}$ responsible for the relaxation of the particles is obtained from:

$$ {g_i}^{eq} = \begin{cases} H - \mathrm{C}_{p,ref}\mathrm{T} + \omega_i \mathrm{C}_p \mathrm{T}\left(\dfrac{\mathrm{C}_{p,ref}}{\mathrm{C}_p} - \dfrac{\boldsymbol{u} \cdot \boldsymbol{u}}{2{c_s}^2} \right) & i = 0 \\ \omega_i \mathrm{C}_p \mathrm{T}\left(\dfrac{\mathrm{C}_{p,ref}}{\mathrm{C}_p} + \dfrac{\boldsymbol{u} \cdot \boldsymbol{c_i}}{{c_s}^2} + \dfrac{(\boldsymbol{u} \cdot \boldsymbol{c_i})^2}{2{c_s}^4} - \dfrac{\boldsymbol{u} \cdot \boldsymbol{u}}{2{c_s}^2} \right) & i \neq 0 \end{cases} \tag{14} $$

where ω_i depends on the selected velocity sets, for example D2Q9 and D2Q5 for two-dimensional analysis and D3Q19 & D3Q7 for three-dimensional analysis obtained from Kruger [8]. To obtain the total macroscopic enthalpy, the zeroth moment of the thermal distribution function is equal to:

$$ H = \sum_{i=0}^{Q-1} g_i(x,t) \tag{15} $$

Consequently, the temperature T and the liquid fraction f_l are obtained by:

$$\mathrm{T}, f_l = \begin{cases} \mathrm{T}_s - \dfrac{H_s - H}{C_{p,s}}, 0 & H < H_s \\ \mathrm{T}_s \left[\dfrac{H_l - H}{H_l - H_s}\right] + \mathrm{T}_l \left[\dfrac{H - H_s}{H_l - H_s}\right], \left[\dfrac{H - H_s}{H_l - H_s}\right] & H_s \leq H \leq H_l \\ \mathrm{T}_L + \dfrac{H - H_l}{C_{p,l}}, 1 & H > H_l \end{cases} \tag{16}$$

The temperature and liquid fraction are dependent on H_s, T_s, $C_{p,s}$, H_l, T_l, and $C_{p,l}$ representing parameters at solidus properties and liquidus properties. The thermophysical properties vary across the phase change. Therefore, the properties are calculated as a function of the properties of the solid and liquid phases. Hung and Wu [9] proposed using reference-specific heat capacity $\left[C_{p,ref} = 2C_{p,s}C_{p,l}/C_{p,l} + C_{p,s}\right]$ for the sake of numerical stability. The above equation corresponds to the harmonic mean of the solid and liquid specific heat capacity to obtain more stable results, as proved by others.

3. Results and Discussion: One-dimensional melting verification

To verify the proposed model and to ensure that the inputs are integrated correctly, the classic one-dimensional Stefan's melting is simulated. Consequently, the obtained results are compared with the analytical solution. The problem consists of melting paraffin wax in a rectangular enclosure initially solid at $t = 0$. The two-dimensional enclosure has a left heating vertical wall with a constant temperature T_h and a right cold vertical wall with a constant temperature T_c. Other walls are set as adiabatic and the PCM at $t = 0$ has a temperature similar to the cold wall as illustrated in Figure 1.

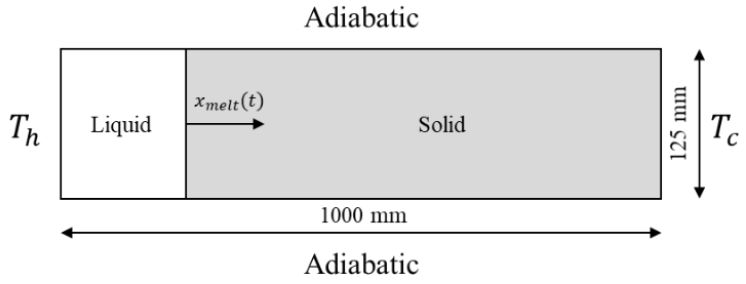

Figure 1 A physical interpretation of conduction melting in an enclosed space. The mushy zone interface is tracked by $x_{melt}(t)$.

At $t > 0$, the melting is initiated, and the interface position and temperature are estimated using Brent's method [10] with the approximation of the melting function φ by Sadoun [11] the equations are given as

$$x_{melt} = 2\varphi\sqrt{\alpha_l t} \tag{17}$$

$$\theta = \frac{T(t) - T_h}{T_c - T_h} = \frac{erf(\,\frac{x}{2}/\sqrt{\alpha_l t}\,)}{erf(\varphi)} \tag{18}$$

$$\varphi = 0.5\sqrt{\sqrt{(Ste + 6)^2 + 24Ste} - (Ste + 6)} \tag{19}$$

Where x_{melt}, φ, θ, $T(t)$ and *Ste* are the position of the melt, melt function, normalized temperature, instantaneous melting temperature, and Stephan's number $\left[Ste = C_{p,l}(T_h - T_c)/L\right]$, respectively.

In this verification, Stephan number is set to 0.01 and the thermal diffusivity is set to 0.1667 m^2/s. The relaxation coefficient is selected as 1.6 with lattice spacing of 7.8 *mm* leading to 128 voxels in the width of the enclosure. Figure 2 illustrates the accuracy of the LBM model compared to the analytical solution for the melt fraction concerning time and the

temperature distribution across the enclosure at different timings. The current LBM model successfully captured the transient behavior of the solid-liquid melting analysis wherein the shift of the mushy interface imitated that of the analytical solution. Moreover, the model achieved accurate thermal performance across the longitudinal distance of the enclosure at various timelines, indicating the potential of the model to handle phase change.

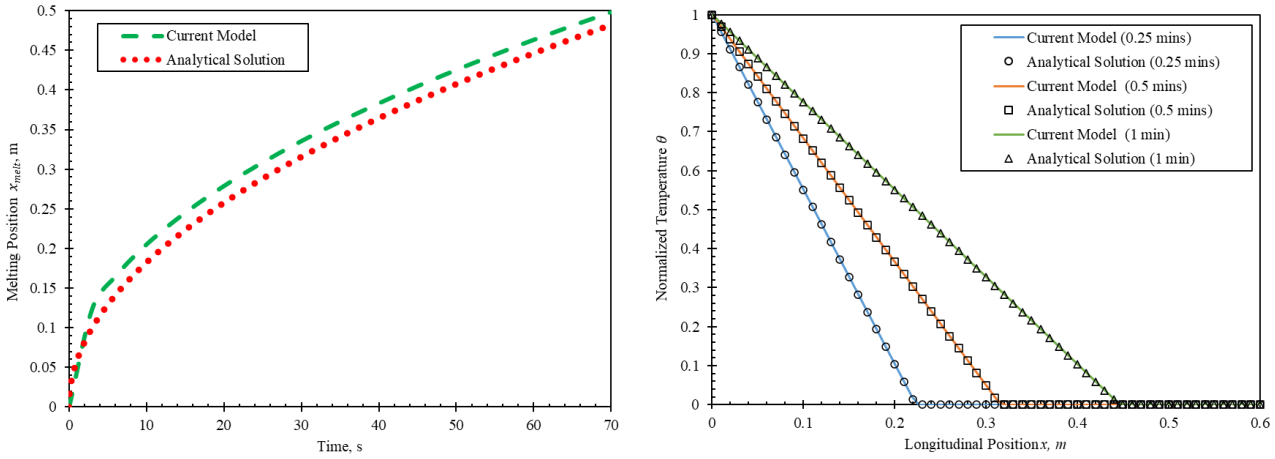

a) b)

Figure 2 a) The plot compares the current LBM solution with the analytical solution in the mushy zone location with respect to time. b) A representation of the normalized temperature distribution of different timings across the whole enclosure in comparison to the findings of the current LBM solution with the analytical solution.

3. Results and Discussion: Two-dimensional melting validation

In contrast to the previous melting case, the mushy zone in an enclosure for this experiment is high enough to start developing an interface that is migrating in both the x and y directions. This phenomenon is essential to mimic since it's more realistic than one-dimensional melting. Therefore, an LBM model is developed for the sake of such validation. The obtained results are compared with the familiar Gau and Viskanta [12] experimental analysis of gallium melting and Brent's [13] numerical approach. The rectangular enclosure has a length of $x = 8.89\,cm$ and a height of $y = 6.35\,cm$ and a width of 3.81 cm. The metal PCM utilized in the study is pure Gallium with a fusion temperature of 302.8 K. The thermophysical properties are summarized in the paper of Brent's [13]. The left hot wall and the right cold wall of the enclosure are taken as 311K and 301.3K. The temperature of the cold wall is selected to be slightly lower than the melting temperature of gallium. Moreover, Other walls are set as adiabatic with bounce-back boundary conditions, as illustrated in Figure 3.

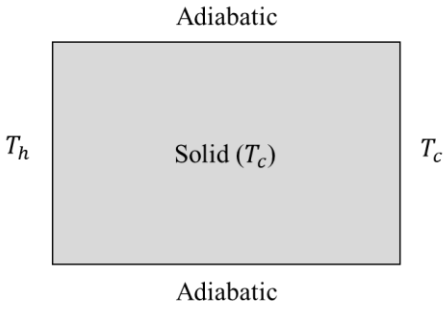

Figure 3 A visual representation of the gallium melting in an enclosure validation.

In the analysis, the relaxation coefficient is set to 0.51, and the grid spacing of each voxel is equal to 0.69 mm. Accordingly, the number of grids in the x direction is 128. The critical dimensionless numbers in this analysis are the Prandtl Prandtl number $[Pr = \upsilon_l/\alpha_l]$, Rayleigh number $\left[Ra = g\beta(T_h - T_c)l_c{}^3/\upsilon_l\alpha_l\right]$, and Stefan's number where l_c is the characteristics length. In this analysis, these nondimensional numbers are set as: Pr $= 0.0216, Ra = 1.656 \cdot 10^6$, and $Ste = 0.039$.

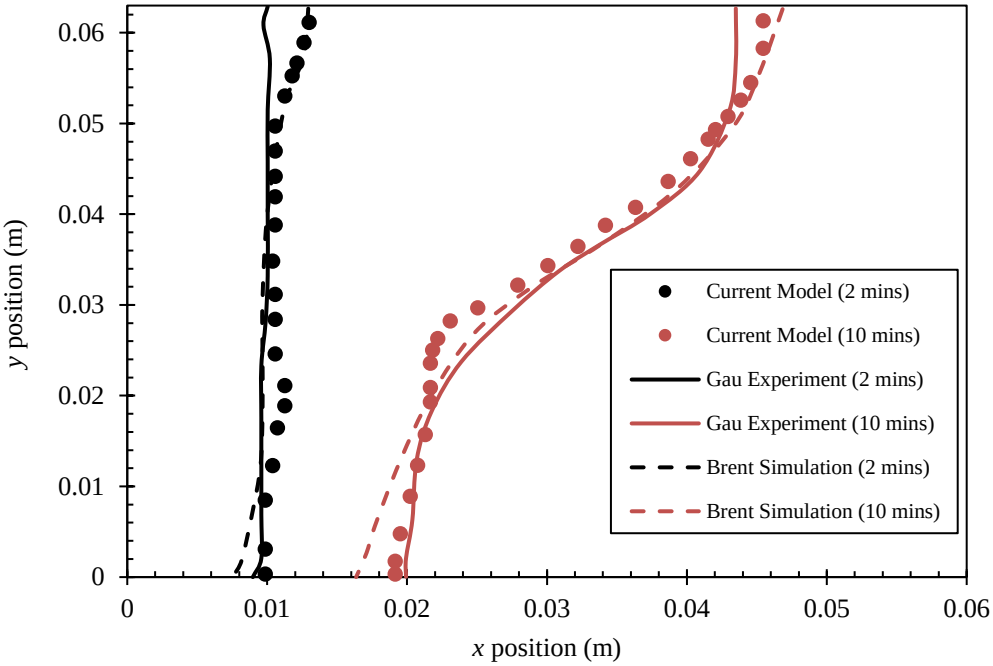

Figure 4 A visual representation of the mushy interface position over *x* and *y* in the timeframes of 2 and 10 minutes. The graph compares the current model with the experimental [12] and numerical [13] works.

According to Figure 4, the LBM model's results are close to the experimental and numerical findings at 2 and 10 minutes. The interface at the first couple of minutes, started shifting away from the heating end in the lateral direction. The deviation of the mushy interface started to appear more in the upper region of the enclosure due to the buoyancy effect where the boundary layer evolves at the hot wall. After the separation of the boundary layer, vortices start to emerge attaining the bubble-shaped interface as shown in the timing of 10 minutes. It can be noted that some deviations from the experimental analysis with the numerical simulation are shown and that originate from the experiment setup and have less to do with the LBM model.

4. Conclusion

In conclusion, this paper aims to establish an optimum thermal management system for cooling high heat-generating electronic devices by implementing phase change material (PCM). However, complicated phenomena such as the melting of phase change material are challenging for conventional Navier-Stokes equation solvers. Therefore, it is necessary to select a suitable computational model capable of dealing with such complexity. Such undertaking is primarily done using the single relaxation enthalpy LB method. To test such a hypothesis, The present models are validated with prominent numerical and experimental studies, for instance, Stefan's conduction melting, and the Gallium melting experiment. These classical analyses provide a comprehensive overview of the performance of the method. The outcomes indicate the complete adaptability of the current model to handle mushy zones during the melting of PCM in both one-dimensional and two-dimensional melting.

Acknowledgments

Our sincere gratitude extends to ASPIRE for their generous funding (AARE20-358), pivotal in realizing our research objectives.

References

[1] G. Moore, "Cramming more components onto integrated circuits," 1965.

[2] Z. Zhang, X. Wang, and Y. Yan, "A review of the state-of-the-art in electronic cooling," *e-Prime - Advances in Electrical Engineering, Electronics and Energy*, vol. 1, p. 100009, Jan. 2021, doi: 10.1016/J.PRIME.2021.100009.

[3] Z. Khattak and H. M. Ali, "Air cooled heat sink geometries subjected to forced flow: A critical review," *Int J Heat Mass Transf*, vol. 130, pp. 141–161, Mar. 2019, doi: 10.1016/J.IJHEATMASSTRANSFER.2018.08.048.

[4] Z. Zhang, X. Wang, and Y. Yan, "A review of the state-of-the-art in electronic cooling," *e-Prime - Advances in Electrical Engineering, Electronics and Energy*, vol. 1, p. 100009, Jan. 2021, doi: 10.1016/J.PRIME.2021.100009.

[5] M. J. Krause *et al.*, "OpenLB—Open source lattice Boltzmann code," *Computers & Mathematics with Applications*, vol. 81, pp. 258–288, Jan. 2021, doi: 10.1016/J.CAMWA.2020.04.033.

[6] D. R. Noble and J. R. Torczynski, "A Lattice-Boltzmann Method for Partially Saturated Computational Cells," *https://doi.org/10.1142/S0129183198001084*, vol. 9, no. 8, pp. 1189–1201, Nov. 2011, doi: 10.1142/S0129183198001084.

[7] R. Huang, H. Wu, and P. Cheng, "A new lattice Boltzmann model for solid–liquid phase change," *Int J Heat Mass Transf*, vol. 59, no. 1, pp. 295–301, Apr. 2013, doi: 10.1016/J.IJHEATMASSTRANSFER.2012.12.027.

[8] T. Krüger, H. Kusumaatmaja, A. Kuzmin, O. Shardt, G. Silva, and E. M. Viggen, "The Lattice Boltzmann Method," 2017, doi: 10.1007/978-3-319-44649-3.

[9] R. Huang and H. Wu, "Phase interface effects in the total enthalpy-based lattice Boltzmann model for solid–liquid phase change," *J Comput Phys*, vol. 294, pp. 346–362, Aug. 2015, doi: 10.1016/J.JCP.2015.03.064.

[10] R. P. Brent, "An algorithm with guaranteed convergence for finding a zero of a function," *Comput J*, vol. 14, no. 4, pp. 422–425, Jan. 1971, doi: 10.1093/COMJNL/14.4.422.

[11] N. Sadoun, E. K. Si-Ahmed, and P. Colinet, "On the refined integral method for the one-phase Stefan problem with time-dependent boundary conditions," *Appl Math Model*, vol. 30, no. 6, pp. 531–544, Jun. 2006, doi: 10.1016/J.APM.2005.06.003.

[12] C. Gau and R. Viskanta, "Melting and Solidification of a Pure Metal on a Vertical Wall," *J Heat Transfer*, vol. 108, no. 1, pp. 174–181, Feb. 1986, doi: 10.1115/1.3246884.

[13] A. D. Brent, V. R. Voller, and K. J. Reid, "ENTHALPY-POROSITY TECHNIQUE FOR MODELING CONVECTION-DIFFUSION PHASE CHANGE: APPLICATION TO THE MELTING OF A PURE METAL," *http://dx.doi.org/10.1080/10407788808913615*, vol. 13, no. 3, pp. 297–318, 2007, doi: 10.1080/10407788808913615.